Feasibility Study of Tumor Size Classification via Contrast-Enhanced UWB Breast Imaging – A Complex-Domain Analysis

S. W. Ahmad[1], Y. Chen[1], P. Kosmas[2], W. L. Woo[1], and S. S. Dlay[1]

[1]School of Electrical, Electronic and Computer Engineering, Newcastle University, Newcastle upon Tyne, NE1 7RU, UK, e-mails: s.w.ahmad@ncl.ac.uk; yifan.chen2@ncl.ac.uk; w.l.woo@ncl.ac.uk; s.s.dlay@ncl.ac.uk
[2]Division of Engineering, King's College London, London WC2R 2LS, UK, e-mail: panagiotis.kosmas@kcl.ac.uk

Abstract

Lesion classification using the tumor's backscatter signature can be very challenging in microwave breast imaging due to the small intrinsic contrast between the dielectric properties of dysplastic and normal tissues. A possible solution to this problem is to use microwave contrast agents such as microbubbles, where the *differential* breast response before and after the administration of the agent to a dysplastic inclusion is used to classify various anomaly properties (size, depth, morphology, etc.). In this paper, we study the feasibility of contrast-agent-aided imaging for lesion size classification by studying received signals in the complex domain. A finite-difference time-domain (FDTD) numerical phantom is employed to simulate electromagnetic (EM) wave propagation inside the breast and extract the reflected waveforms with and without microbubbles in the tumor site. The complex-domain transfer function of differential response is then used to draw the poles-zero plots (PZPs) and Bode plots (BPs), which demonstrate the viability of the proposed method for lesion size categorization.

1. Introduction

There have been considerable efforts in recent years to investigate the possibility of using microwave technology for early-stage breast cancer detection and lesion classification [1]–[9]. An important objective of applying microwave methods to breast imaging is to determine the tumor size, which is related to the stage of cancer development. However, this approach is greatly challenged by the small intrinsic contrast between the dielectric properties of tumor and its surrounding tissues, which has been recently reported in a large-scale breast tissue dielectric-spectroscopy study [10]. According to this study, the dielectric properties of benign tissues are similar to those of lower-adipose-content normal breast tissues, and the contrast in the dielectric properties between malignant and normal glandular/fibroconnective tissues (non-adipose) is no more than about 10%. As nearly all breast cancers originate within glandular tissues, a malignant tumor will be a weakly scattering target within a highly cluttered environment. This would lead to severe deterioration of lesion size classification.

The problem could be possibly overcome by administering contrast agents such as dielectric or conducting micro/nano-particles into a dysplastic site, similar to other recent feasibility studies in contrast-enhanced microwave imaging [4], [5], [7]. This approach could provide comparative information for tissue size classification through dynamic monitoring of backscatter signature over time. Recent preliminary studies have suggested that the dielectric properties of a tumor are altered in the presence of microbubbles [4], [11] or single-walled carbon nanotubes [7]. In this paper, we study the feasibility of using contrast agents to determine the size of a lesion by analyzing the differential backscatter before and after administration of contrast agents to the cancerous site in the complex domain. Both the pole-zero plots (PZPs) and Bode plots (BPs) are utilized for this purpose.

The rest of the paper is organized as follows. In Section 2, the methodology and specification for simulations are described. In Section 3, the simulation results are presented. Finally, some concluding remarks are drawn in Section 4.

2. Methodology

A two-dimensional (2D) finite-difference time-domain (FDTD) model as shown in Fig. 1 is used for the numerical simulation of electromagnetic (EM) wave propagation in the breast medium, where the perfectly matched layer (PML) absorbing boundary condition (ABC) [12] is employed to improve the system dynamic range and reduce reflections from the boundaries. The whole simulation space comprises 100×100 cells in the xy-plane. The resolution of the grid is 3 mm/cell with a time step of 7.07×10^{-12} seconds. The excitation wave is a modulated Gaussian pulse, $\exp\left(-t^2/\tau^2\right)\sin\left(2\pi ft\right)$, where $\tau = 1$ ns defines the width of the ultra-wideband (UWB) pulse and $f = 5$ GHz.
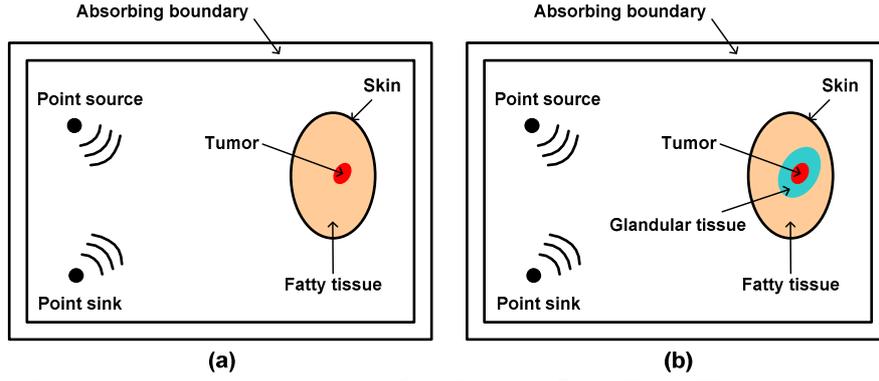
Figure 1. Numerical breast phantoms for (a) Case I and (b) Cases II and III considered in this study.

The breast phantom is modeled as an ellipse with a major axis of 18.6 cm and a minor axis of 11.7 cm as shown in Fig. 1. The skin thickness is 3.3 mm. The glandular tissue is modeled as an ellipse with a major axis of 6.3 cm and a minor axis of 4.8 cm as shown in Fig. 1(b). Furthermore, three different sizes of the tumor with major axes of 20 mm, 15 mm, 10 mm, and minor axes of 16 mm, 12 mm, and 8 mm are considered. Note that in all the following discussions, we will use (α, β) to indicate the size of an ellipse with α and β being the major and minor axes, respectively.

We employ a transverse electric (TE) EM wave, and study three different cases. In Case I, the tumor is surrounded by fatty breast tissues comprising only high-adipose contents (see also Fig. 1(a)). In Case II, the tumor is embedded in low-adipose glandular tissues, and no contrast agent is applied at this stage. Finally, Case III corresponds to the same model as in Case II, Fig. 1(b), but this time we assume that microbubbles have been infused into the cancerous site and differential imaging is utilized.

The relative permittivity and conductivity for the skin, fatty tissues, glandular tissues, and tumor are assumed to be 34.5, 4.2, 40, 43.6, and 4.5 S/m, 0.16 S/m, 5 S/m, 6.94 S/m, respectively For Case III we assume that the microbubbles reduce the tumor's relative permittivity to 34.9, corresponding to 20% dielectric reduction as suggested in [4], and reduce the tumor's conductivity to 4.5 S/m. Although far from being realistic, these breast and tumor models can serve as a testbed for an initial assessment of our proposed method.

3. Simulation Results

The rational transfer function for the imaging systems shown in Fig. 1 is given by,

$$H(z) = \frac{B(z)}{A(z)} = \frac{b[0]z^0 + b[1]z^{-1} + b[2]z^{-2} + \cdots + b[n]z^{-n}}{a[0]z^0 + a[1]z^{-1} + a[2]z^{-2} + \cdots + a[n]z^{-n}} \tag{1}$$

where $A(z)$ is the z-transform of the incident UWB signal. In Cases I and II, $B(z)$ represents the reflected waveform after subtracting the skin response, while in Case III it denotes the differential backscatter, which is defined as the difference between the post-contrast and pre-contrast breast responses.

Subsequently, the PZPs of (1) can be obtained. Fig. 2(a) illustrates the PZPs for three different sizes of tumors in Case I, where circles represent zeros and crosses represent poles. Apparently, all the poles are located within the unit circle, which demonstrates the stability of the imaging system. Moreover, a significant shift in the locations of zeros can be registered as the tumor size varies. At first sight, the variation seems to be quite random. Nevertheless, a more regular phenomenon emerges in the BPs shown in Fig. 2(b), where the phase of $H(z)$ decreases over the entire normalized frequency range as the tumor size decreases.

Next, the PZPs and BPs for Case II are shown in Fig. 3. Due to the significant clutter interference caused by glandular tissues, both plots fail to demonstrate any noticeable change in either the zero locations (Fig. 3(a)) or the Bode magnitude and phase diagrams (Fig. 3(b)). Subsequently, the PZPs and BPs for Case III when the differential imaging technique is applied are depicted in Fig. 4. Similar to Fig. 2(a), a noticeable variation in the zero locations can be observed in Fig. 4(a) as the tumor size varies. Furthermore, the tumor size has a strong impact on the phase of $H(z)$ over the whole frequency range as shown in Fig. 4(b), following the same trend as the one identified in Fig. 2(b). Finally, Fig. 5 presents a closer view of the Bode phase plots in Fig. 4(b). Spikes immediately after the constant phase stage can be found as shown in the encircled regions in Fig. 5. It can be seen that tumors of different sizes lead to different patterns and strengths of these spikes, which may provide additional insight into the problem of tumor size categorization.
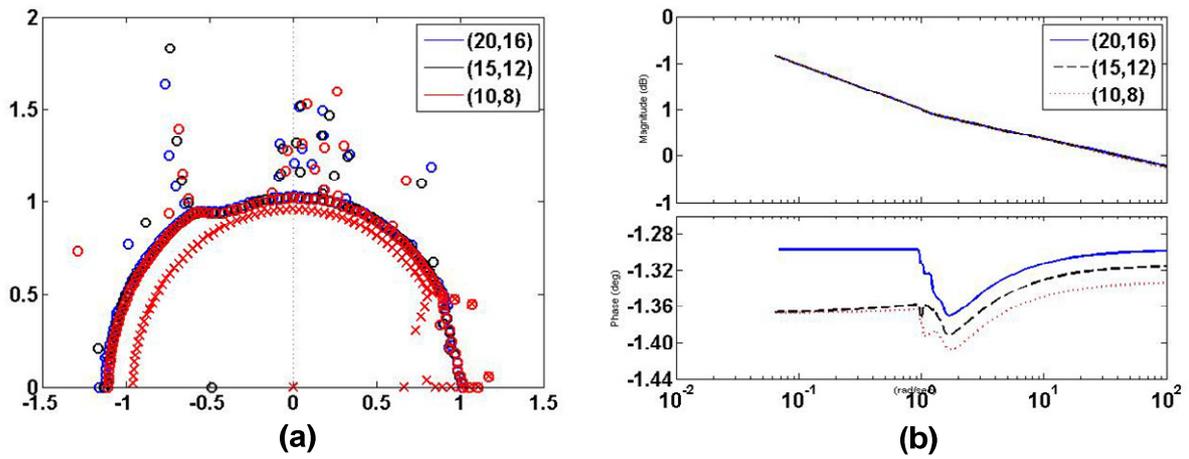
Figure 2. (a) Pole-zero plots (PZPs) and (b) Bode plots (BPs) for Case I (Fig. 1(a)). In (a), significant shift in the zero locations can be registered as the tumor size varies. In (b), the phase of $H(z)$ decreases as the tumor size decreases.
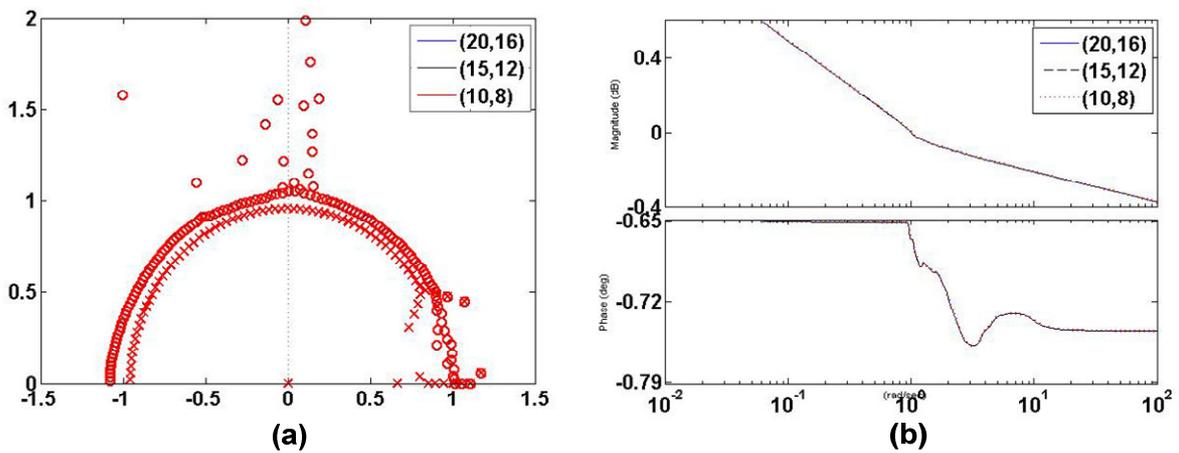

Figure 3. (a) PZPs and (b) BPs for Case II (Fig 1(b) and no contrast agent), which fail to demonstrate any noticeable change in the zero locations or the Bode diagrams.
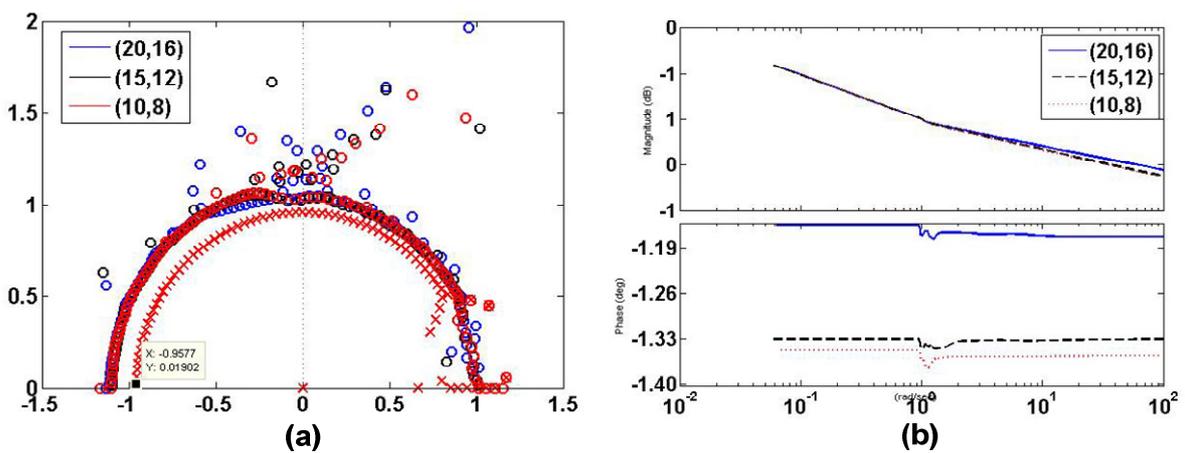

Figure 4. (a) PZPs and (b) BPs for Case III (Fig 1(b) and differential contrast-enhanced data). In (a), significant shift in the zero locations can be registered as the tumor size varies. In (b), the phase of $H(z)$ decreases as the tumor size decreases.
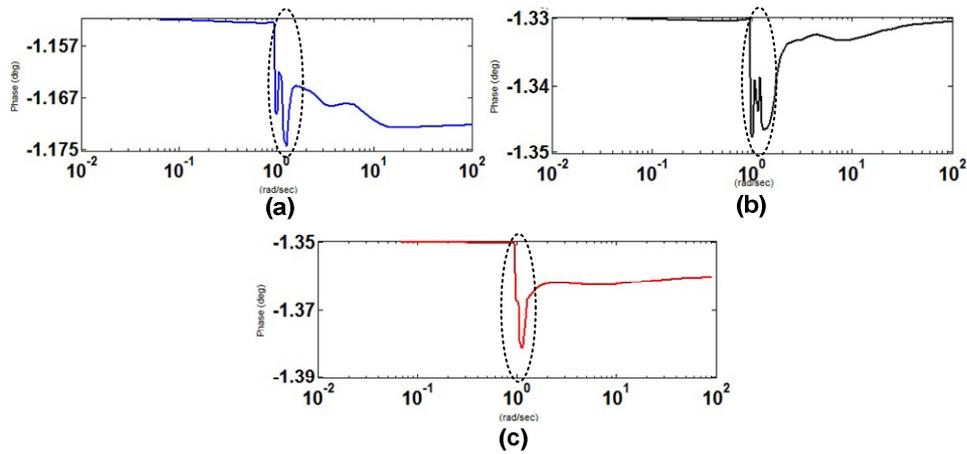
Figure 5. Zoomed-in Bode phase plots in Fig. 4(b) for different tumor sizes: (a) (20 mm, 16 mm), (b) (15 mm, 12 mm), and (c) (10 mm, 8 mm). Tumors of different sizes lead to different patterns of the spikes in the encircled regions.

4. Conclusion

This paper presents a new technique for lesion classification via contrast-enhanced microwave breast imaging, based on analyzing the transfer function of the incident and reflected breast responses. We have attempted to classify the sizes of tumors by observing the locations of zeros in the PZPs and the phase in the BPs with simplified breast models, which produce strong clutter noise due to surrounding low-adipose glandular tissues. The following additional cases are currently under investigation to further substantiate the observations made in this work: (i) employing more realistic numerical breast phantoms; (ii) considering more examples for various tumor sizes; and (iii) categorizing other lesion properties such as depth and morphology. The technique could also be combined with other recent methods used for discrimination of malignant tumors from benign lesions [1], [6], [9].

7. References

[1] Y. Chen, E. Gunawan, K. S. Low, S.-C. Wang, C. B. Soh, and T. C. Putti, "Effect of lesion morphology on microwave signature in 2-D ultrawideband breast imaging," *IEEE Trans. Biomed. Eng.*, vol. 55, no. 8, pp. 2011–2021, Aug. 2008.

[2] P. Kosmas and C. M. Rappaport, "A matched-filter FDTD-based time reversal approach for microwave breast cancer detection," *IEEE Trans. Antennas Propag.*, vol. 54, no. 4, pp. 1257–1264, Apr. 2006.

[3] J. M. Sill and E. C. Fear, "Tissue sensing adaptive radar for breast cancer detection—Experimental investigation of simple tumor models," *IEEE Trans. Microw. Theory Tech.*, vol. 53, no. 11, pp. 3312–3319, Nov. 2005.

[4] A. Mashal, J. H. Booske, and S. C. Hagness, "Toward contrast-enhanced microwave-induced thermoacoustic imaging of breast cancer: An experimental study of the effects of microbubbles on simple thermoacoustic targets," *Phys. Med. Biol.*, vol. 54, pp. 641–650, 2009.

[5] J. D. Shea, P. Kosmas, S. C. Hagness, and B. D. Van Veen, "Contrast enhanced microwave breast imaging," presented at the *13th Int. Symp. Antenna Technol. Appl. Electromagn. Can. Radio Sci. Meet.*, Edmonton, AB, Canada, Feb. 2009.

[6] Y. Chen, I. J. Craddock, P. Kosmas, M. Ghavami, and P. Rapajic, "Multiple-input multiple-output radar for tissue classification in ultra-wideband breast imaging," *IEEE J. Select. Topics Signal Processing*, Special Issue on MIMO Radar and Its Applications, vol. 4, no. 1, pp. 187-201, 2010.

[7] A. Mashal, B. Sitharaman, J. H. Booske, and S. C. Hagness, "Dielectric characterization of carbon nanotuble contrast agents for microwave breast cancer detection," presented at the *IEEE Int. Symp. Antennas Propag. (APS)*, Charleston, SC, Jun. 2009.

[8] D. A. Woten, J. Lusth, and M. El-Shenawee, "Interpreting artificial neural networks for microwave detection of breast cancer," *IEEE Microw. Wireless Compon. Lett.*, vol. 17, no. 12, pp. 825–827, Dec. 2007.

[9] S. K. Davis, B. D. Van Veen, S. C. Hagness, and F. Kelcz, "Breast tumor characterization based on ultrawideband microwave backscatter," *IEEE Trans. Biomed Eng.*, vol. 55, no. 1, pp. 237246, Jan. 2008.

[10] M. Lazebnik, D. Popovic, L. McCartney *et al.*, "A large-scale study of the ultrawideband microwave dielectric properties of normal, benign and malignant breast tissues obtained from cancer surgeries," *Phys. Med. Biol.*, vol. 52, pp. 6093–6115, 2007.

[11] O. Ogunlade, Y. Chen, and P. Kosmas, "Measurement of the complex permittivity of microbubbles using a cavity perturbation technique for contrast enhanced ultra-wideband breast cancer detection," presented at the *IEEE EMBC 2010*, Buenos Aires, Argentina, Aug. 31-Sept. 4, 2010.

[12] J. P. Berenger, "A perfectly matched layer for the absorption of electromagnetic wave," *Journal of Computational Physics*, vol. 114, no. 2, pp. 185-200, 1994.